Polymer Testing 106 (2022) 107463

Contents lists available at ScienceDirect

Polymer Testing

journal homepage: www.elsevier.com/locate/polytest

Towards a consistent methodology for testing the electromechanical performance of strip polymer composite actuators

Yuqing Dong [a], Ka-Wai Yeung [a], Wing-Cheung Law [a], Gary Chi-Pong Tsui [a], Xiaolin Xie [b], Chak-Yin Tang [a,*]

[a] Department of Industrial and Systems Engineering, The Hong Kong Polytechnic University, Hong Kong, China
[b] School of Chemistry and Chemical Engineering, Huazhong University of Science and Technology, Wuhan, Hubei, 430074, China

ARTICLE INFO

Keywords:
Actuator
Bending evaluation
Interpolation
Least-square method

ABSTRACT

Strip actuators have attracted tremendous attention in bionics due to the controllable deformation under various stimuli. However, it is currently hard to compare their performance owing to the different approaches for evaluating their actuation. Most of the studies determine the maximum or average value of the bending angle or strain, the deformation profile of the entire actuator strip was not quantified. In this study, a versatile method was proposed to evaluate the bending profile of typical strip actuators with bending deformation, thus analyzing the actuation performance. This method has been verified by synthetic curves, and less than 2% of global error was found. We have also demonstrated the implementation of this method for examining the actuation of typical strip actuators and showed that it can also be used for comparing the performance of different actuators prepared from other studies.

1. Introduction

Polymeric smart actuators have attracted a lot of research attention due to their great potential in the fields of wearable flexible electronics, artificial muscles, and advanced MEMS devices [1–3]. Generally, these actuators are used as energy transducers that convert external physical or chemical stimuli into large mechanical deformations such as shrinkage, expansion, and bending [4–6]. The most typical actuation behavior for strip- or flat-structural actuators is bending, which is a two-dimensional deformation involving changes in the internal structure or composition of the actuators [6]. Evaluating the actuation performance is of great importance to the structure or material optimization and the design of the actuators, especially for the bending deformation of strip actuators.

Many approaches have been taken to evaluate the bending performance of strip actuators. Tip displacement or deflection, which is closely related to the length of the actuator, is a common and simple method to describe the bending of an actuator [7,8]. However, the magnitude of the displacement is usually insufficient to describe the bending behavior of the entire sample. The bending angle is also used to characterize the deformation. Generally, the bending angle is defined as the angle between the starting point and the endpoint of the actuated sample relative to the original position [9] or the tangent at the end of the strip actuator bending section [10,11]. When the bending only involves a part of the sample strip or when curling occurs, the measurement of tangent could be a more reasonable approach [12]. Qu et al. [13] reported a porous actuator composed of graphene oxide (GO) and cellulose acetate (CA) that reached a maximum bending angle of 720°, with a helical shape in acetone vapor. A similar strip actuator composed of carbon and CA was also fabricated and showed a more irregular bending under the same stimulation conditions. In this case, it is difficult to quantitatively describe and compare the performance of these two actuators using the bending angle. Similar problems were also found in oil-triggered actuators composed of silicone rubber and graphene [14]. Lou et al. [15] developed a polytetramethylene glycol-based double-layer strip actuator that bent under chloroform vapor and a maximum angle of 180° was reported, and the actuator could be cut and spliced into a more complex strip owing to its self-healing function. A changeable wave-shaped bending deformation was achieved. In this case, however, the bending angle may not be accurate enough to present the deformation of the entire sample strip.

Curvature (κ) and bending strain (ε) are also widely used to characterize the bending deformation of strip actuators in terms of different parameters such as the bending angle, tip displacement, and thickness of

* Corresponding author. Department of Industrial and Systems Engineering, The Hong Kong Polytechnic University, Hung Hom, Kowloon, Hong Kong, China.
E-mail address: cy.tang@polyu.edu.hk (C.-Y. Tang).

https://doi.org/10.1016/j.polymertesting.2021.107463
Received 31 August 2021; Received in revised form 8 December 2021; Accepted 27 December 2021
Available online 29 December 2021

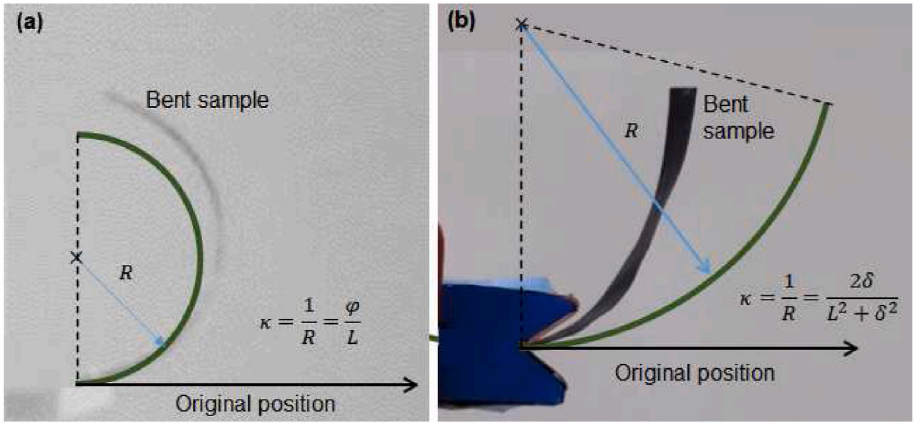

Fig. 1. Typical approaches for calculating the average curvature of strip actuators. (a) a moisture-responsive actuator with a length of 15 mm, and an average curvature of 3.1 cm^{-1} [16] (Reprinted (adapted) with permission from Copyright (2017) The Royal Society of Chemical); (b) a potential-responsive actuator with a length of 25 mm, and an average curvature of 0.38 cm^{-1} [17] (Reprinted (adapted) with permission from Copyright (2021) Wiley-VCH). The equivalent arcs with the same calculated curvature of the sample are presented in green color. (For interpretation of the references to color in this figure legend, the reader is referred to the Web version of this article.)

the bent sample [16–18]. Generally, the approaches for calculating the curvature of strip actuators are usually determined by assuming the bent actuator fits an arc of a circle and thus calculating the bending strain by the product of the sample curvature and its thickness [19]. Therefore, obtaining accurate curvature data of a strip actuator is particularly important when characterizing its bending deformation. Fig. 1(a) demonstrates one of the approaches to calculate the curvature of a strip actuator by dividing the tangent angle (φ) at the free end of the actuator by its original length (L) [16,20]. One of the limitations for this calculation is that the actual length of the sample may vary during the actuation process. This may lead to an inaccurate result of the actual curvature of the sample [20]. Another approach, as illustrated in Fig. 1 (b), has been widely used to assess the performance of strip actuators such as ionic electroactive polymers (iEAP) [21,22] and Bucky gel actuators [23,24]. By measuring the tip displacement (δ) and the length of the actuator (L), the curvature of the sample was calculated [17,18]. However, due to the different measurement methods of L in different studies, the calculated bending strain between the same type of actuator may still not be directly comparable. Moreover, as the bent actuator does not always fit an arc of a circle perfectly, it may not satisfy the initial assumption of the calculation. This results in a significant deviation between the equivalent arcs of the calculated curvature (green arcs in Fig. 1) and the sample.

Evaluating the curvature distribution, or angular deflection per unit length, along the entire length of the strip actuator, is a rational method to estimate its bending performance [25]. By quantifying the curvature distribution, other useful information such as the homogeneity of the strip material could also be identified. However, it is mathematically complicated to evaluate this parameter of a complex curve. Software such as Kappa in ImageJ has been developed to calculate the curvature of a given curve. Kappa is a semi-automatic curve fitting tool based on the cubic Bézier curve, which subdivides the fitted curve through the *de Casteljau* algorithm and uses a simple endpoint formula to evaluate the curvature iteratively. However, this method is highly dependent on the curve fitting process [26]. Therefore, problems such as over-fitting usually occur for low-order and complex curves because the control points used in curve fitting are usually added and moved manually, which may lead to inaccurate results.

In this study, we proposed a consistent method for evaluating the bending performance of strip actuators. By analyzing the image of the bent actuator using Matlab, an accurate fitting of the curved actuator can be undertaken and the corresponding curvature distribution of the entire actuator is obtained. In addition, it is possible to compare the overall actuation properties of the same type of actuator by calculating their average curvature based on the curvature distribution results. With the assistance of Matlab, the bending behavior of different iEAPs can be calculated and compared. We also demonstrated a comparative study between different actuators of the same type using the proposed method,

Table 1
Common methods to evaluate the bending deformation of strip actuators.

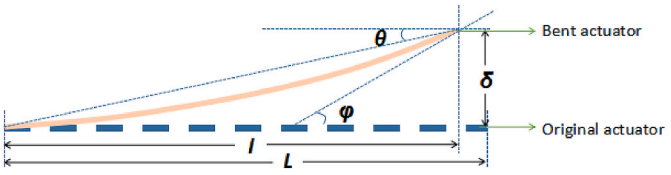

Parameters	
Tip displacement	δ [7,8]
Bending angle	θ [9]
	φ [10,11]
Average curvature	φ/L [16]
Bending strain	$2d\delta/(L^2+\delta^2)$ [17]
	$2d\delta/(l^2+\delta^2)$ [18]

where d is the thickness of the strip actuator.

analyzing the effect of the controlling factors, such as actuator size, stimulation voltage, ions type, and internal structure which is crucial for the design and optimization of a strip actuator. The curvature distribution and average curvature would provide a reference for the improvement of the structure and components of the actuators.

2. Experiment

A typical iEAP was prepared, and the proposed method was applied to fit our samples and iEAPs from other reports. Thus, the actuation response of those iEAPs with different sizes and components under different voltages was compared.

2.1. Materials

Polyvinyl alcohol (PVA, polymerization degree 1750) was obtained from Sinopharm Group, China. Ionic liquid (1-Decyl-3-methylimidazolium Chloride, C_{10}MIMCl) was purchased from IoLiTec, Germany. The gold foil (thickness, 110 nm) was purchased from Ouci Metal, China.

2.2. Preparation of iEAP

The electrolyte solution was prepared by mixing 0.5 g PVA and 0.25 g C_{10}MIMCl in 9.25 mL DI water and stirring for more than 5 h at 95 ° C. The electrolyte membrane was prepared by casting 2 g of the above solution into a Petri dish and allowing the solvent to evaporate at room

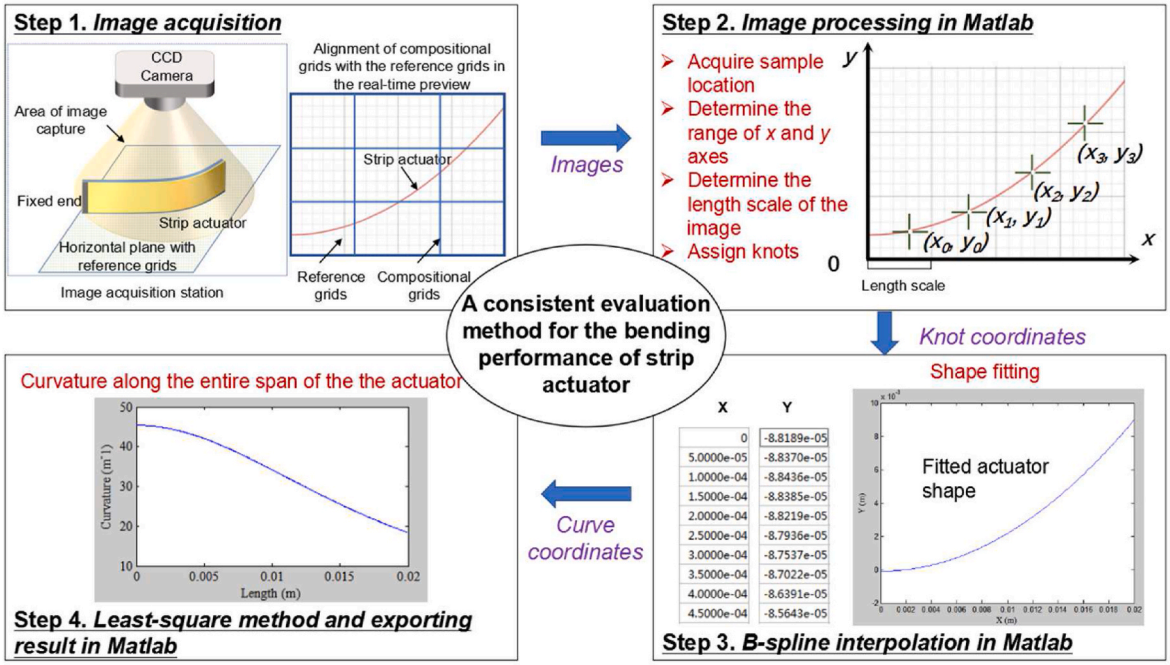

Fig. 2. Procedure of the proposed evaluation method for the performance of strip actuators.

temperature. Gold foils were attached to both sides of the PVA/IL electrolyte membrane to prepare an iEAP sample of a size of 30 mm × 3 mm × 0.1 mm.

2.3. Bending performance evaluation

Typical evaluation methods for the actuation performance of strip actuators, which include the measurement of tip displacement, bending angle, average curvature, and bending strain, are summarized in Table 1. These evaluation results can be influenced by the bending mechanism and size of the sample, even if the same method is used. For example, neither the tip displacement (δ) nor bending angle (θ) can accurately describe the deformation of an actuator that only deforms locally. In addition, some reports used different measurements for calculating the average curvature, such as the original length L or projected length l after bending, leading to the results not being comparable. Therefore, a consistent evaluation method for describing the actuation behavior is crucial, so as to provide a comparable and accurate bending performance of the same type of actuator, thereby improving the component or structural design of the actuator.

A method is proposed to evaluate the bending performance of a strip actuator more consistently by calculating the curvature distribution based on B-spline interpolation and the least-square method. The evaluation procedure, including the image acquisition, processing, and shape fitting of a strip actuator, is illustrated in Fig. 2. First, an image acquisition station is used to record the deflection of the strip actuator with illumination (Fig. 2, step 1). The CCD camera is fixed above a horizontal plane with reference grids and connected with a computer. The real-time preview feature of the CCD camera allows the computer screen to be used as a viewfinder for framing. The orientation of the camera is adjusted to ensure the parallelism between the CCD sensor of the camera and the horizontal plane. This can be done by aligning the compositional grids displayed in the real-time computer preview with the reference grids of the horizontal plane. To minimize drift or distortion of the image, the strip actuator is required to be placed at the center of the area of capture, and its cross-section in the thickness direction should be orthogonal to both the horizontal plane and the CCD sensor. In this way, the influence of gravity on its deflection output can be reduced, and the image of true shape of the strip actuator can be captured. The acquired image of the actuator is then imported into Matlab for shape fitting.

In the image processing (Step 2), a Cartesian plane is first located. The fixed end of the actuator is placed on the y-axis, and the original shape of the actuator is along the positive x-axis of the Cartesian plane. The orientation of the actuator does not influence the curvature distribution results. The length scale of the Cartesian plane can be determined using the reference grids with a known size. Then, the sampling points, or knots, are allocated along the curved contour of the strip actuator for the B-spline interpolation. The interpolation method used in the proposed study is cubic B-spline, thereby a minimum of 4 knots is required when fitting an unknown curve, which is demonstrated in detail in the principle of fitting calculation. For curves with complex shapes, $m+1$ knots are needed, where m is the number of the circular arc segments taken to approximate the curve [27]. The positions of the knots are recommended to select as a uniform knot vector [28,29], especially for monotonic and symmetrical curves. In addition, for periodic curves, the number and positions of nodes can be assigned periodically according to the shape of the unit curve. The details of the influence of the number of knots on the curvature fitting result can be found in the supporting information. After obtaining the knot coordinates, the cubic B-spline interpolation method is applied to fit the curved shape of the entire actuator (Step 3). B-spline interpolation method is an efficient fitting tool that is commonly applied to obtain smooth fitted curves. It connects the knots in a continuous second derivative to ensure the curve smoothness and accuracy of the fitted results [30]. The coordinates of the fitted curve are also generated with the B-spline fitting process. Then, the angular deflection per unit length along the entire span of the actuator can be calculated using the least-square method based on these coordinates (Step 4). The circular regression equation is performed on the continuous n fitting coordinates to calculate the corresponding curvature. The influence of n value on the curvature fitting result is mentioned in supporting information. This fitting process is semi-automatic and only required users to determine the number and position of knots. This can provide a reliable basis for the comparison and analysis of actuator performance. For dynamic measurement, the bending motion captured with an appropriate frame rate can be processed similarly.

Extracting accurate and continuous points of the target strip actuator

is important in evaluating its curvature through the least-square method. B-spline interpolation was applied to fit points based on the selected knots on the curve, to obtain smoothed curve and plane coordinates. The B-spline interpolation is a numerical method that can allow the interpolation function to show an overall smoothness without relying on a known derivative [30]. The final fitted curve passes through each knot to ensure fitting precision. The general B-spline interpolation fitting and curvature calculation processes for a given curve are summarized as follows:

1 The boundary with the size of the curve to be fitted is first determined, and $n+1$ ($n \geq 2$) points are randomly selected on the curve for interpolation calculation. Then, a spline function in each data interval $[x_i, x_{i+1}]$ can be defined as:

$$S_i(x) = a_i(x-x_i)^3 + b_i(x-x_i)^2 + c_i(x-x_i) + d_i,\ i = 0,\ 1,\ \ldots, n-1 \tag{1}$$

Thus, a total of $4n$ known conditions are required to obtain the corresponding. parameters of each function.

2. Each $S_i(x)$ is continuous in each interval, that is:

$$S_i(x_i) = y_i,\ S_i(x_{i+1}) = y_{i+1},\ i = 0,\ 1, \ldots, n-1; \tag{2, 3}$$

$$S'_{i-1}(x_i) = S'_i(x_i),\ i = 1,\ 2,\ \ldots, n-1; \tag{4}$$

$$S''_{i-1}(x_i) = S''_i(x_i),\ i = 1,\ 2,\ \ldots, n-1. \tag{5}$$

with natural boundary conditions:

$$S''_0(x_0) = y''_0 = 0,\ S''_n(x_n) = y''_n = 0 \tag{6}$$

3. The second derivative value of the piecewise spline function $S_i(x)$ is assumed as:

$$M_i = S''_i(x),\ i = 0,\ 1,\ \ldots, n-1 \tag{7}$$

Then, M_i is a linear function in each interval. Each $S_i(x)$ can be obtained after integrating twice with two boundary conditions:

$$S_i(x) = \frac{(x_i - x)^3}{6h_i}M_{i-1} + \frac{(x - x_{i-1})^3}{6h_i}M_i + \left(y_{i-1} - \frac{M_{i-1}h_i^2}{6}\right)\frac{x_i - x}{h_i} + \left(y_i - \frac{M_i h_i^2}{6}\right)\frac{x - x_{i-1}}{h_i} \tag{8}$$

where $h_i = x_i - x_{i-1}$ is the step size.

4. For all intervals, the equations about M_{i-1}, M_i, M_{i+1} are obtained after sorting:

$$\alpha_i M_{i-1} + 2M_i + \beta_i M_{i+1} = g_i\ ,\ i = 1,\ 2, \ldots, n-1 \tag{9}$$

Here,

$$\alpha_i = \frac{h_i}{h_i + h_{i+1}}, \tag{10}$$

$$\beta_i = 1 - \alpha_i, \tag{11}$$

$$g_i = \frac{6}{h_i + h_{i+1}}\left(\frac{y_{i+1} - y_i}{h_{i+1}} - \frac{y_i - y_{i-1}}{h_i}\right). \tag{12}$$

5. The coefficient matrix is strictly diagonally dominant and invertible, and can be solved with a unique solution:

$$\begin{bmatrix} 2 & 1 & & & \\ \alpha_1 & 2 & \beta_1 & & \\ \alpha_2 & 2 & \beta_2 & & \\ & \ddots & \ddots & \ddots & \\ & \alpha_{n-1} & 2 & \beta_{n-1} & \\ & & 1 & 2 & \end{bmatrix}\begin{bmatrix} M_0 \\ M_1 \\ M_2 \\ \vdots \\ M_{n-1} \\ M_n \end{bmatrix} = \begin{bmatrix} g_0 \\ g_1 \\ g_2 \\ \vdots \\ g_{n-1} \\ g_n \end{bmatrix} \tag{13}$$

6. For N points $P_i \in (X_i,\ Y_i)$, $i = 1,\ 2,\ 3, \ldots, N$ fitted by B-spline interpolation, the least-square circle fitting calculation is performed for every consecutive *3* points (Fig. S1), that is,

$$minS(a,b,c) = \sum_i^{i+2}\left[X_i^2 + Y_i^2 + aX_i + bY_i + c\right]^2 \tag{14}$$

where $minS(a,b,c)$ is the minimized sum of the squared differences on both sides of the equal sign. By solving equation (15), the curvature of the fitted circle can be obtained as:

$$\kappa = \frac{1}{R} = \frac{2}{\sqrt{a^2 + b^2 - 4c}} \tag{15}$$

and the average global error E_k is computed as:

$$E_k = \frac{\sum\left|\left(\rho_{t(k)} - \rho_k\right)W_k\right|}{|Q|} \tag{16}$$

where $\rho_{t(k)}$ and ρ_k are the theoretical and fitted curvature at each point, W_k is the. weight for each point, and $|Q|$ is the number of data points collected in Matlab.

7. The average curvature is calculated by the following equations. Thus, the overall deformation of iEAPs with different lengths is comparable.

$$\kappa = \frac{1}{R} = \frac{d\varphi}{dL} \tag{17}$$

$$Ave_\kappa = \frac{\int_0^L \kappa dL}{L} \tag{18}$$

where φ is the deflection angle, and L is the length of the iEAP sample.

B-spline interpolation is a common fitting tool for computer-aided design, image processing, and signal processing. It was reported as a useful and effective method for fitting low-resolution images with a better Peak Signal-to-Noise ratio [31]. It was utilized for fitting noisy spectrum data to produce a smoother result and minimize data distortion, which is more reliable as compared to the convolution method [32]. In this work, the curved actuator image was captured by a high-resolution CCD camera (a pixel resolution of 4032×3024), and then the knots were taken on the curve for interpolation calculation. To verify the accuracy of B-spline interpolation, synthetic curves with a minimum pixel resolution of 360×300 were used, and the error in the fitting results did not exceed 2%. Therefore, the image resolution has minimal effect on the accuracy of the curve fitting and curvature results, which ensures the reliability of the proposed method. In addition, the proposed method offers a quantitative way to describe the bending deformation of strip actuators by calculating curvature distribution and average curvature, and also considering the length difference before and after actuation.

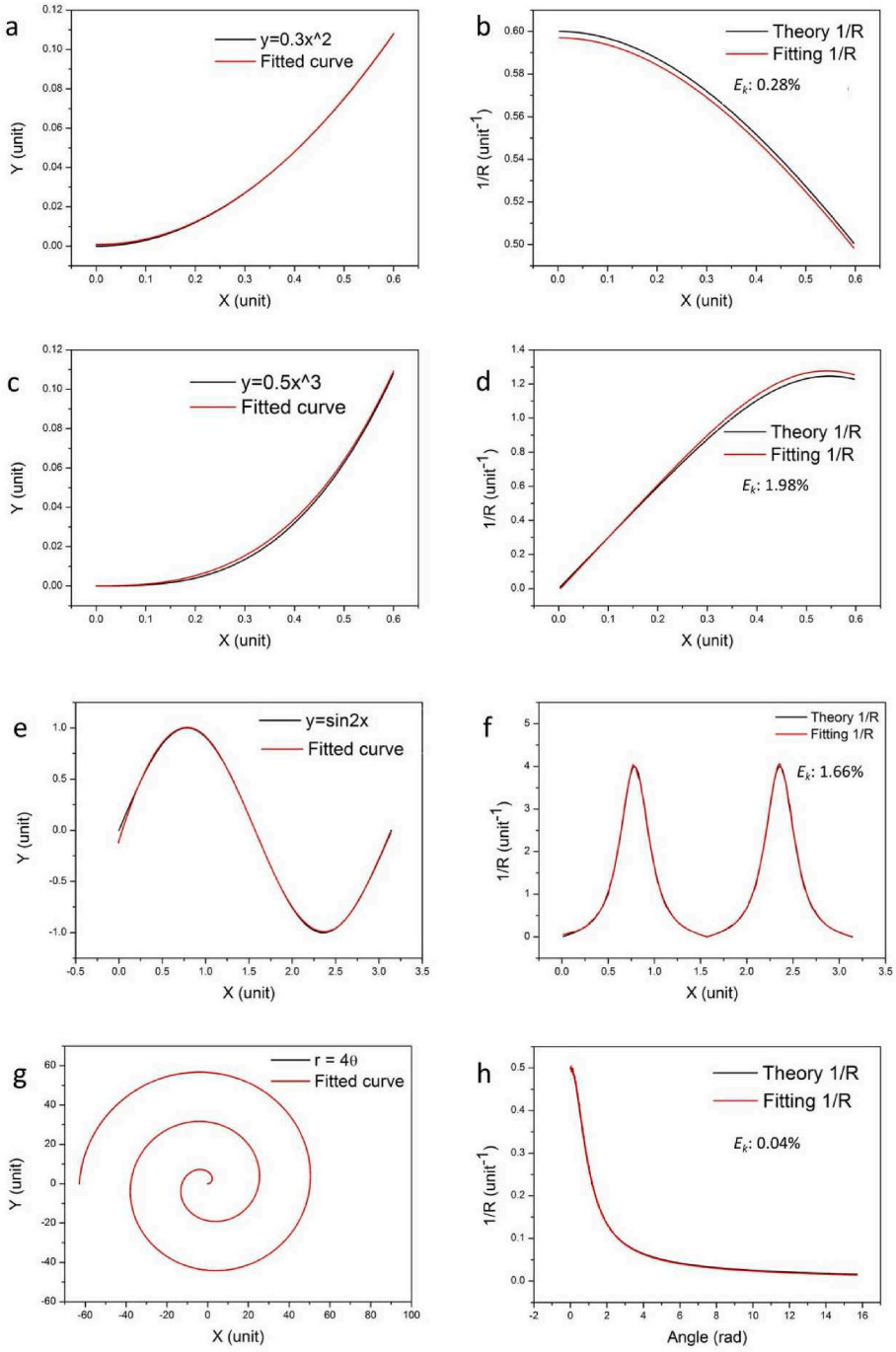

Fig. 3. Curve and curvature fitting results of typical curves including (a–b) $y = 0.3x^2$ ($x \in [0,0.06]$); (c–d) $y = 0.5x^3$ ($x \in [0,0.06]$); (e–f) $y = sin2x$ ($x \in [0, \pi]$); (g–h) $r = 4\theta$ ($\theta \in [0, 5\pi]$).

3. Results and discussion

3.1. Validation of the proposed method

To demonstrate the applicability of the proposed method, it was implemented to calculate the curvature distribution of different synthetic curves, including the power function, trigonometric function, and Archimedes spiral, which showed a similar shape with the bending response of most strip actuators [33,34]. The typical synthetic curves and their curve fitting results, curvature, and average global error are illustrated in Fig. 3. It can be observed that the B-spline interpolation results in a good fitting with an average global error of less than 2% for the curves without periodicity on the abscissa, such as power functions and wave functions. For different power functions with similar shapes, their theoretical curvatures might be completely different. For example, as shown in Fig. 3(a–d), similar curve shapes but different curvature distributions were found in the segments of $y = 0.3x^2$ and $y = 0.5x^3$ ($x \in [0, 0.6]$). The spline interpolation results in well fitting for curves with different orders only according to the knots (Fig. 3(a, c)), and the minimum fitting accuracy was only 0.28% for the low-order curve. Trigonometric functions also provide good verification cases because of the uniqueness of the periodicity of the curve. As illustrated in Fig. 3(e), the shape of the sine curve was generally fitted with only a slight difference within the interval $\left[0, \frac{\pi}{2}\right]$. Correspondingly,

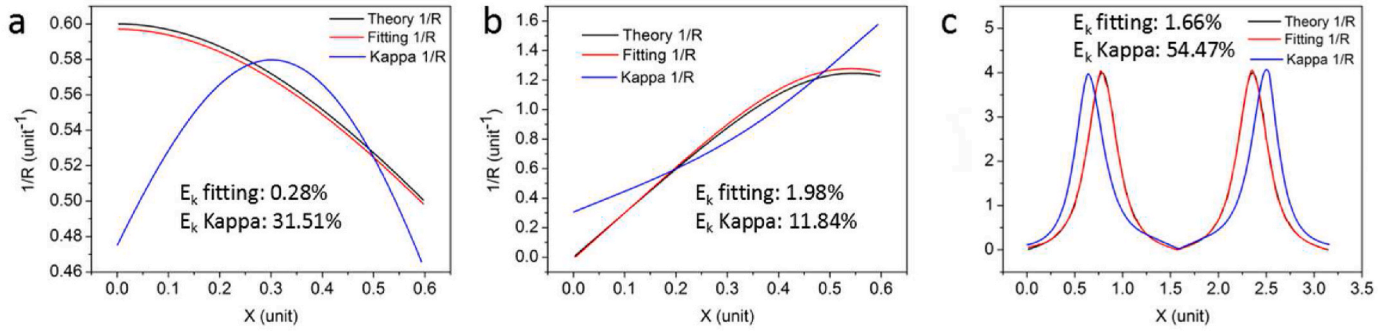

Fig. 4. The curvature results calculated by Kappa and the least square method. (a) $y = 0.3x^2$ ($x \in [0, 0.6]$); (b) $y = 0.5x^3$ ($x \in [0, 0.6]$); (c) $y = sin2x$ ($x \in [0, \pi]$).

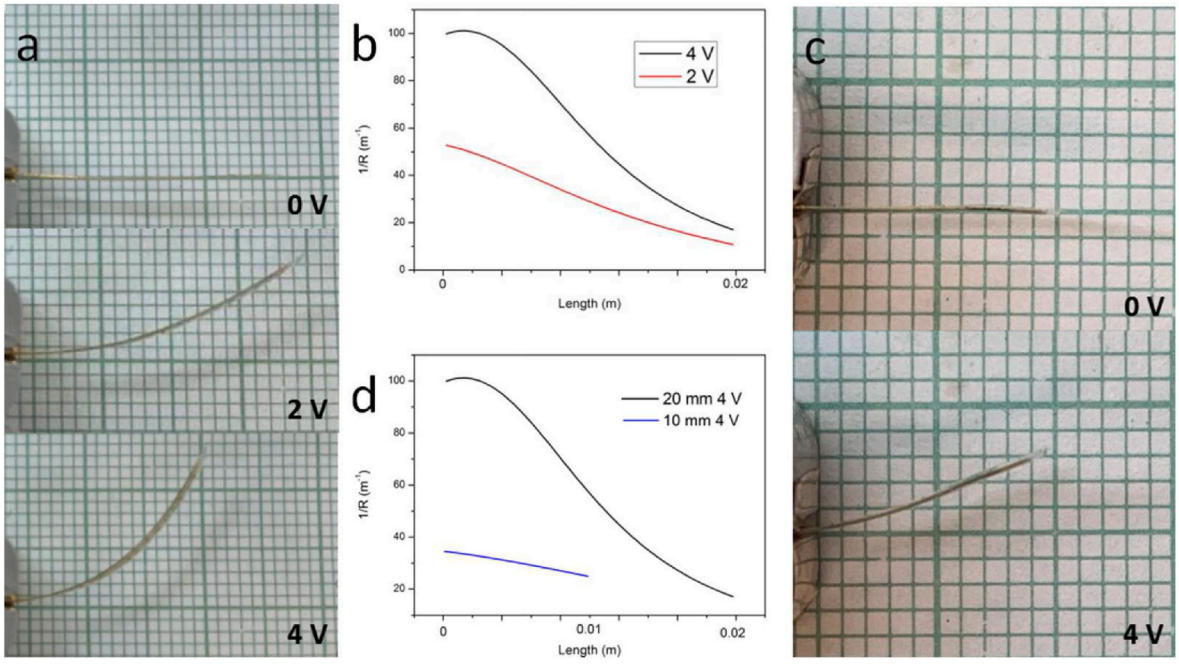

Fig. 5. (a) Bending response and (b) curvature distribution of iEAP composed of PVA/C_{10}MIMCl and gold foil with a length of 20 mm under 2 V and 4 V; (c) bending response and (d) curvature distribution of the same iEAP (10 mm) under 4 V. (For interpretation of the references to color in this figure legend, the reader is referred to the Web version of this article.)

the main difference in the curvature fitting results was also observed in the same interval, and the final error was 1.66%. Spiral deformation is common for vapor responsive actuators with long free lengths [13,14]. Due to the uneven point density of the spiral, an additional spiral fitting algorithm is required to obtain a smooth curve. The fitted spiral was found to almost overlap with the original spiral curve, and the average global error of the fitted curvature was only 0.04% (Fig. 3(g and h)).

As mentioned above, Kappa exhibits large errors when calculating low-order curves. For instance, as shown in Fig. 4(a), the resulting curvature distribution as calculated using Kappa significantly deviated from the theoretical value for the segment of $y = 0.3x^2$ ($x \in [0, 0.6]$), with an error of 31.51%. When fitting a cubic curve $y = 0.5x^3$ ($x \in [0, 0.6]$), the curvature distribution calculated by Kappa also showed an increasing trend. However, the corresponding error was shown to be as high as 11.84% (Fig. 4(b)). Moreover, the accuracy of Kappa in fitting the trigonometric function is related to the image resolution. More accurate curvature fitting results can be obtained from an image with a higher resolution after Kappa processing [19]. One of the advantages of fitting the curve directly through the B-spline is that the number of interpolation points can be adjusted according to the actual curve length, and it does not rely on the image resolution. Although the fitted curvature result of the sine curve in Kappa showed a similar shape to the theoretical curvature, the value had shifted, resulting in a much greater error (54.47%) as compared to the B-spline interpolation processing (error of 1.66%) (Fig. 4(c)). The large errors of Kappa curve fitting can be ascribed to its automatic connection of the control points with cubic Bézier curves, resulting in over-fitting. Compared with Kappa curve fitting, B-spline interpolation offers a more reliable and robust approach for fitting curves without considering their orders or resolution.

3.2. Bending performance of iEAPs

The iEAP usually exhibits an uneven bending response due to its composition, internal structure, size, and actuation voltage. Here, we demonstrate the application of the proposed method as an evaluation tool for the bending performance of strip actuators. The deformation images of the as-prepared iEAP composed of PVA/IL electrolyte membrane and gold electrodes were collected, processed, and calculated in Matlab to analyze the bending response along the length of the sample using the proposed method.

As shown in Fig. 5(a), the free end length of this iEAP was 20 mm. Due to the high continuity and low resistivity of the gold foil electrodes,

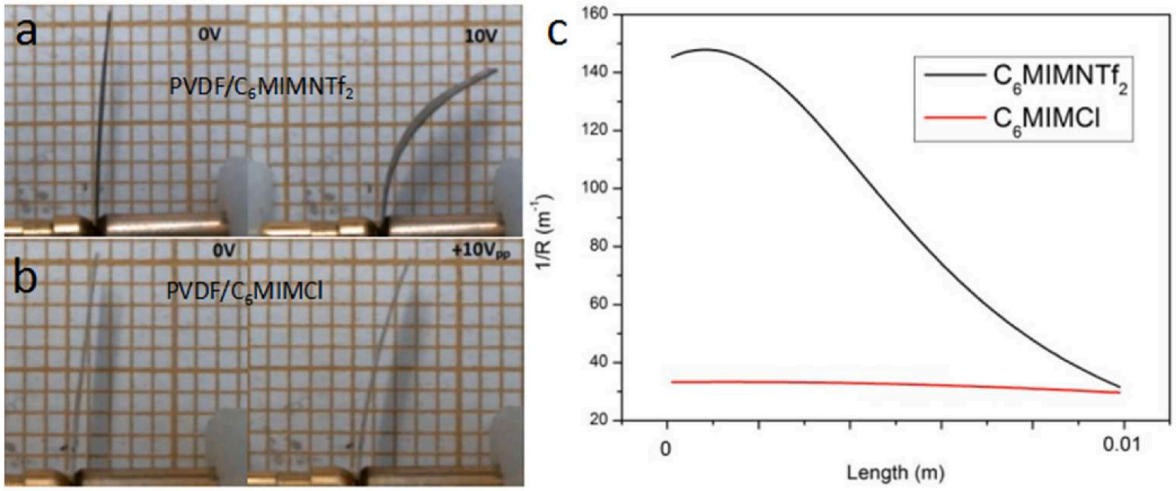

Fig. 6. Bending deformation of iEAPs composed of electrolyte membrane (a) PVDF/C_6MIMNTf$_2$ [36] (Reprinted (adapted) with permission from Copyright (2016) Elsevier) and (b) PVDF/C_6MIMCl [35] with gold electrodes under 10 V (Reprinted (adapted) with permission from Copyright (2016) Elsevier); (c) curvature distribution of two kinds of iEAPs along their lengths. (For interpretation of the references to color in this figure legend, the reader is referred to the Web version of this article.)

the iEAP showed obvious bending under a voltage of only 2 V. The largest curvature was as high as 52.7 m^{-1}, which was found in the part close to the contact electrode, that is, the starting position of the bent sample. The average curvature at 2 V also reached 29.650 m^{-1}. As the actuation voltage was increased to 4 V, the corresponding maximum curvature was up to 101.1 m^{-1}, which was almost twice that under 2 V stimulation. In addition, the average curvature reached 58.280 m^{-1}, showing an increase of 96.56% as compared to the result with 2 V stimulation (Fig. 5(b)). The difference was that the highest curvature of the sample at 4 V was observed at the position about 10% of the length from the contact electrode. This can be ascribed to the effect of accumulating deformation under a slightly higher actuation voltage. The sample length was also one of the factors influencing actuation performance. As shown in Fig. 5(c and d), the highest curvature was 33.2 m^{-1} at 4 V when the length of the iEAP of the same composition was only 10 mm. And the average curvature was 29.198 m^{-1}, which is much smaller than that of iEAP with a length of 20 mm.

We also employed our method to evaluate the bending performance of the reported strip actuators using the imidazole-type IL. For example, Mejri et al. [35,36] prepared two kinds of blended electrolyte membranes composed of polyvinylidene fluoride (PVDF) and ionic liquids 1-hexyl-3-methyl imidazolium bis(trifluoromethylsulfonyl)imide (C_6MIMNTf$_2$), and (1-hexyl-3-methylimidazolium chloride (C_6MIMCl), respectively, with sputter-coated gold contact electrodes on the surfaces to fabricate iEAPs. The anion of the ionic liquid was reported to be advantageous for adjusting the phase and crystallinity of the PVDF, thereby reducing the mechanical properties of the electrolyte membrane [37]. The PVDF/C_6MIMNTf$_2$ iEAP with lower crystallinity showed a maximum bending curvature of 147.8 m^{-1} under 10 V and a 0.1 Hz square wave voltage stimulation (Fig. 6(a)). A short-term superimposing effect of the bending behavior emerged close to the contact electrode, which resulted in a slow increase in its curvature distribution. Similar to the bending behavior of the iEAP as-prepared in our work, as the resistance of the surface gold electrodes increased, the curvature distribution decreased rapidly along the direction of the iEAP away from the contact electrode. The curvature of the ends of both iEAPs was only around 30 m^{-1}. The average curvatures of the two iEAPs also exhibited a large difference. The PVDF/C_6MIMCl iEAP sample with higher mechanical properties showed an average curvature of 31.537 m^{-1} (Fig. 6 (b)), which was only 34.71% of the PVDF/C_6MIMNTf$_2$ iEAP sample. The results show good agreement with those reported in the literature [35, 36].

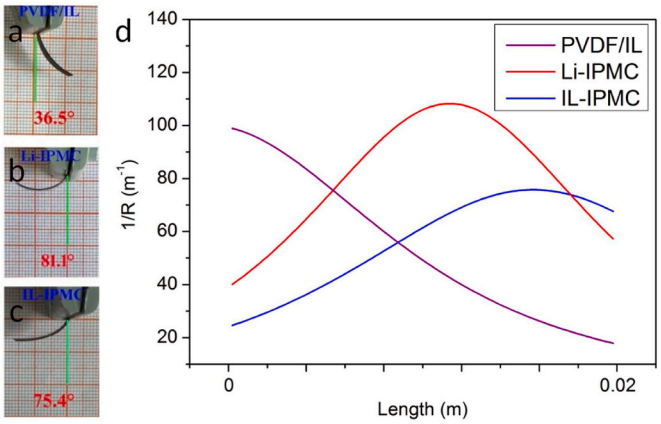

Fig. 7. Bending deformation of iEAPs constituted of electrolyte membrane (a) PVDF/IL (EMIBF$_4$), (b) Nafion/Li^+, and (c) IL-IPMC (PVDF/PVP/EMIBF$_4$) with graphite electrodes under 15 V [9] (Reprinted (adapted) with permission from Copyright (2019) American Chemical Society); (d) curvature distribution of iEAPs along their lengths.

The IL-based iEAP usually faces the problem of ions migration. Due to the large molecular size and high viscosity of ILs, this type of iEAP generally exhibits slower and lower saturation bending under DC voltage as compared to the iEAPs containing inorganic ions. Guo et al. [9] reported three different iEAPs based on Li^+ and IL (1-Ethyl-3--methylimidazolium tetrafluoroborate, EMIBF$_4$) in studying the effect of ions mobility on the bending angle. The bending behavior and curvature distribution of the iEAPs are presented in Fig. 7. It was found from the curvature analysis that these iEAPs exhibit completely different bending performances. Although the initial curvature of the PVDF/IL iEAP (Fig. 7 (a)) was the largest (99.8 m^{-1}), it decreased quickly along its length until the end (20 m^{-1}). Inorganic ions migrated more easily in the electrolyte because of their smaller size and lower viscosity, and the corresponding curvature showed a trend that increased and then decreased (Fig. 7(b)), and its largest curvature was close to 110 m^{-1}. By sacrificing a water-soluble template (PVP) in the PVDF membrane to increase the internal migration channels of ILs, the new iEAP (Fig. 7(c)) exhibited a bending behavior like Li-IPMC and was ascribed to more ions migrate to the corresponding electrode, resulting in an iEAP with a gradually increasing curvature. Although IL-IPMC (Fig. 7(c)) with inner migration

Table 2
Average curvature of iEAPs with different compositions and sizes.

iEAP Electrolyte membrane		Electrode	Length (mm)	Actuation voltage (V)	Average curvature (m^{-1})	References
Polymer	Ions					
PVA	C_{10}MIMCl	Gold	20	2	29.650	This work
				4	58.280	
			10	4	29.198	
PVDF	C_6MIMCl	Gold	10	10	31.537	[35]
	C_6MIMNTf_2				90.860	[36]
PVDF	$EMIBF_4$	Graphite	20	15	52.495	[9]
Nafion	Li^+				80.265	
PVDF/PVP	$EMIBF_4$				55.330	

channels had a larger bending angle and a different curvature distribution as compared to the original sample (Fig. 7(a)), their average curvature differed only by 2.835 m^{-1}. Moreover, they were both much smaller than the Li^+ containing iEAP samples.

By implementing the proposed method, the overall actuation performance of iEAPs with different sizes and compositions can be obtained, which is very beneficial when employing the proposed method for comparative studies. The material composition, actuation condition, actuator size, and the average curvature of the above-mentioned works are summarized in Table 2. In general, the bending performance of an iEAP with the same material composition increases with the increase in its length, which is consistent with the results reported by Guo et al. [38]. In the works reported here, as the length of PVA/C_{10}MIMCl iEAP decreased from 20 mm to 10 mm, the corresponding average curvature at 4 V was reduced by 49.9% to only 29.198 m^{-1}. The PVDF/C_6MIMCl iEAP with a length of 10 mm had an average curvature of 31.537 m^{-1} at 10 V. As compared to the PVA-based iEAP, its curvature was only increased by 8.01% but the actuation voltage was increased by 150%. In addition, as NTf_2^- showed a larger effect on reducing the crystallinity and mechanical properties of the PVDF membrane [36], a 2.88 times increase in the average curvature was calculated for the PVDF/C_6MIMNTf_2 iEAP as compared to PVDF/C_6MIMCl iEAP. As compared with the work reported by Guo et al. [9], even though the ion migration channel was enhanced by the novel fabrication method, the average curvature of the PVDF/PVP/$EMIBF_4$ iEAP at 15 V (55.330 m^{-1}) was lower than that of the PVA-based iEAP at 4 V (58.280 m^{-1}). In addition, the IL used in this work has longer alkyl chains, thus a higher viscosity compared with $EMIBF_4$. The advantages of the PVA/IL iEAP may be attributed to the low crystallinity of the polymer matrix, the hygroscopicity of the ionic liquid, and the large difference in ion sizes. Further investigation is required for a better understanding of the underlying actuation mechanism. Thus, we have demonstrated the implementation of the proposed method as an effective tool for comparing the bending behavior of different strip actuators.

4. Conclusions

In this paper, we have presented a consistent method based on B-spline interpolation and least squares regression analysis, to calculate the bending behavior of a strip actuator with the aid of Matlab. The proposed method was verified by synthetic curves and was showed to effectively overcome the limitations of the other curvature calculation software, such as Kappa in ImageJ. A low fitting error of less than 2% was achieved for fitting low-order and wave curves. The bending profiles of different iEAP actuators were obtained by using the proposed method, and their bending performances were analyzed. In addition, this method can also be used for the comparison of different strip actuators, providing a consistent methodology for testing.

Author statement

Chak-yin Tang: Conceptualization, Supervision, Methodology, Project Administration, Writing – review & editing. **Yuqing Dong:** Methodology, Investigation, Analysis, Writing – original, Writing – review & editing. **Ka-Wai Yeung:** Methodology, Investigation, Analysis, Writing – original, Writing – review & editing. **Wing-Cheung Law:** Supervision, Methodology, Writing – review & editing. **Gary Chi-Pong Tsui:** Writing - review & editing. **Xiaolin Xie:** Methodology, Writing - review & editing.

Declaration of competing interest

The authors declare that they have no known competing financial interests or personal relationships that could have appeared to influence the work reported in this paper.

Acknowledgment

The work described in this paper was fully supported by a grant from the Research Grants Council of the Hong Kong Special Administrative Region, China (Project No. PolyU 15200318).

Appendix A. Supplementary data

Supplementary data to this article can be found online at https://doi.org/10.1016/j.polymertesting.2021.107463.

References

[1] X. Yu, H. Cheng, M. Zhang, Y. Zhao, L. Qu, G. Shi, Graphene-based smart materials, Nat. Rev. Mater. 2 (2017) 1–13, https://doi.org/10.1038/natrevmats.2017.46.
[2] M.A. English, L.R. Soenksen, R.V. Gayet, H. de Puig, N.M. Angenent-Mari, A. S. Mao, P.Q. Nguyen, J.J. Collins, Programmable CRISPR-responsive smart materials, Science 365 (2019) 780–785, https://doi.org/10.1126/science.aaw5122.
[3] R. Kumar, A. Sharma, H. Singh, P. Suating, H.S. Kim, K. Sunwoo, I. Shim, B.C. Gibb, J.S. Kim, Revisiting fluorescent calixarenes: from molecular sensors to smart materials, Chem. Rev. 119 (2019) 9657–9721, https://doi.org/10.1021/acs.chemrev.8b00605.
[4] L. Chen, Y. Dong, C.-Y. Tang, L. Zhong, W.-C. Law, G.C. Tsui, Y. Yang, X. Xie, Development of direct-laser-printable light-powered nanocomposites, ACS Appl. Mater. Interfaces 11 (2019) 19541–19553, https://doi.org/10.1021/acsami.9b05871.
[5] Q. Zhang, M. Wang, H. Ao, H. Luo, X. Deng, Y. Wan, Embedding carbon nanotube to the surfaces of poly (ε-caprolactone) film for multi-responsive actuations, Polym. Test. 96 (2021) 107086, https://doi.org/10.1016/j.polymertesting.2021.107086.
[6] C. Zheng, F. Jin, Y. Zhao, M. Zheng, J. Liu, X. Dong, Z. Xiong, Y. Xia, X. Duan, Light-driven micron-scale 3D hydrogel actuator produced by two-photon polymerization microfabrication, Sensor. Actuator. B Chem. 304 (2020) 127345, https://doi.org/10.1016/j.snb.2019.127345.
[7] L. Chen, C. Liu, K. Liu, C. Meng, C. Hu, J. Wang, S. Fan, High-performance, low-voltage, and easy-operable bending actuator based on aligned carbon nanotube/polymer composites, ACS Nano 5 (2011) 1588–1593, https://doi.org/10.1021/nn102251a.
[8] S. Degeratu, G. Subțirelu, A. Rotaru, N. Bîzdoacă, P. Rotaru, The electro-mechanical control of element NiTi shape memory alloy strip while bending, based on thermal analysis evidence, J. Therm. Anal. Calorim. 143 (2021) 3805–3815, https://doi.org/10.1007/s10973-020-10172-5.
[9] D. Guo, Y. Han, J. Huang, E. Meng, L. Ma, H. Zhang, Y. Ding, Hydrophilic poly (vinylidene fluoride) film with enhanced inner channels for both water-and ionic liquid-driven ion-exchange polymer metal composite actuators, ACS Appl. Mater. Interfaces 11 (2019) 2386–2397, https://doi.org/10.1021/acsami.8b18098.

[10] L. Dong, X. Tong, H. Zhang, M. Chen, Y. Zhao, Near-infrared light-driven locomotion of a liquid crystal polymer trilayer actuator, Mater. Chem. Front. 2 (2018) 1383–1388, https://doi.org/10.1039/C8QM00190A.
[11] G. Wang, H. Xia, X.-C. Sun, C. Lv, S.-X. Li, B. Han, Q. Guo, Q. Shi, Y.-S. Wang, H.-B. Sun, Actuator and generator based on moisture-responsive PEDOT: PSS/PVDF composite film, Sensor. Actuator. B Chem. 255 (2018) 1415–1421, https://doi.org/10.1016/j.snb.2017.08.125.
[12] A. Punning, K.J. Kim, V. Palmre, F. Vidal, C. Plesse, N. Festin, A. Maziz, K. Asaka, T. Sugino, G. Alici, Ionic electroactive polymer artificial muscles in space applications, Sci. Rep. 4 (2014) 1–6, https://doi.org/10.1038/srep06913.
[13] J. Qu, F. Gao, J. Zhao, L. Duan, Y. Zang, S. Wen, Graphene oxide/polymer actuator driven by acetone vapor enabling an ultra-large bending angle and fast response, Smart Mater. Struct. 28 (2019) 105043, https://doi.org/10.1088/1361-665x/ab3c2e.
[14] Z.-P. Yu, L.-M. Dong, Y.-Y. Song, Y.-J. Shi, Y. Liu, A controllable oil-triggered actuator with aligned microchannel design for implementing precise deformation, Nanoscale 12 (2020) 15426–15434, https://doi.org/10.1039/d0nr03157g.
[15] J. Lou, Z. Liu, L. Yang, Y. Guo, D. Lei, Z. You, A new strategy of discretionarily reconfigurable actuators based on self-healing elastomers for diverse soft robots, Adv. Funct. Mater. 31 (2021) 2008328, https://doi.org/10.1002/adfm.202008328.
[16] L. Chen, M. Weng, P. Zhou, L. Zhang, Z. Huang, W. Zhang, Multi-responsive actuators based on a graphene oxide composite: intelligent robot and bioinspired applications, Nanoscale 9 (2017) 9825–9833, https://doi.org/10.1039/C7NR01913K.
[17] F. Wang, Q.-C. Li, J. Park, S.-h Zheng, E. Choi, Ultralow voltage high-performance bioartificial muscles based on ionically crosslinked polypyrrole-coated functional carboxylated bacterial cellulose for soft robots, Adv. Funct. Mater. 31 (2021) 2007749, https://doi.org/10.1002/adfm.202007749.
[18] N. Terasawa, Self-standing high-performance transparent actuator based on poly (dimethylsiloxane)/TEMPO-Oxidized cellulose nanofibers/ionic liquid gel, Langmuir 36 (2020) 6154–6159, https://doi.org/10.1021/acs.langmuir.0c00559.
[19] A.P. Boresi, R.J. Schmidt, O.M. Sidebottom, Advanced Mechanics of Materials, Wiley New York, 1985. Advanced mechanics of materials.
[20] C. Fang, K. Yang, Q. Zhou, K. Peng, H. Yang, A monolithic anti-freezing hydro/organo Janus actuator with sensitivity to the polarity of solvents, RSC Adv. 8 (2018) 35094–35101, https://doi.org/10.1039/C8RA06719H.
[21] F. Lu, T. Chen, K. Xiang, Y. Wang, Ionic electro-active polymer actuator based on cobalt-containing nitrogen-doped carbon/conducting polymer soft electrode, Polym. Test. 84 (2020) 106413, https://doi.org/10.1016/j.polymertesting.2020.106413.
[22] F. Wang, Q. Li, J.O. Park, S. Zheng, E. Choi, Ultralow voltage high-performance bioartificial muscles based on ionically crosslinked polypyrrole-coated functional carboxylated bacterial cellulose for soft robots, Adv. Funct. Mater. (2020) 2007749, https://doi.org/10.1002/adfm.202007749.
[23] T. Fukushima, K. Asaka, A. Kosaka, T. Aida, Fully plastic actuator through layer-by-layer casting with ionic-liquid-based bucky gel, Angew. Chem. Int. Ed. 44 (2005) 2410–2413, https://doi.org/10.1002/anie.200462318.
[24] K. Mukai, K. Asaka, K. Kiyohara, T. Sugino, I. Takeuchi, T. Fukushima, T. Aida, High performance fully plastic actuator based on ionic-liquid-based bucky gel, Electrochim. Acta 53 (2008) 5555–5562, https://doi.org/10.1016/j.electacta.2008.02.113.
[25] Q. Pei, O. Inganäs, Electrochemical applications of the bending beam method. 1. Mass transport and volume changes in polypyrrole during redox, J. Phys. Chem. 96 (1992) 10507–10514. https://pubs.acs.org/doi/pdf/10.1021/j100204a071.
[26] H. Mary, G.J. Brouhard, Kappa (κ): analysis of curvature in biological image data using B-splines, bioRxiv (2019) 852772, https://doi.org/10.1101/852772.
[27] A. Razdan, Knot Placement for B-Spline Curve Approximation 1.7, Arizona State University, Tempe, AZ, 1999, p. 8. Knot placement for B-spline curve approximation.
[28] W.Y. Ma, J.P. Kruth, Parameterization of randomly measured points for least squares fitting of B-spline curves and surfaces, Comput. Aided Des. 27 (9) (1995) 663–675, https://doi.org/10.1016/0010-4485(94)00018-9.
[29] L.A. Piegl, W. Tiller, Least-squares b-spline curve approximation with arbitary end derivatives, Eng. Comput. 16 (2) (2000) 109–116, https://doi.org/10.1007/PL00007188.
[30] C. De Boor, A Practical Guide to Splines, Springer-Verlag, New York, 1978. A practical guide to splines.
[31] M.Z. Hussain, S. Abbas, M. Irshad, Quadratic trigonometric B-spline for image interpolation using GA, PLoS One 12 (6) (2017), e0179721, https://doi.org/10.1371/journal.pone.0179721.
[32] M.H. Zhu, L.G. Liu, D.X. Qi, Z. You, A.A. Xu, Least square fitting of low resolution gamma ray spectra with cubic B-spline basis functions, Chin. Phys. C 33 (1) (2009) 24. https://iopscience.iop.org/article/10.1088/1674-1137/33/1/006/meta.
[33] W. MohdIsa, A. Hunt, S.H. HosseinNia, Sensing and self-sensing actuation methods for ionic polymer–metal composite (ipmc): a review, Sensors 19 (2019) 3967, https://doi.org/10.3390/s19183967.
[34] D. Guo, L. Wang, X. Wang, Y. Xiao, C. Wang, L. Chen, Y. Ding, PEDOT coating enhanced electromechanical performances and prolonged stable working time of IPMC actuator, Sensor. Actuator. B Chem. 305 (2020) 127488, https://doi.org/10.1016/j.snb.2019.127488.
[35] R. Mejri, J. Dias, S.B. Hentati, G. Botelho, J. Esperança, C. Costa, S. Lanceros-Mendez, Imidazolium-based ionic liquid type dependence of the bending response of polymer actuators, Eur. Polym. J. 85 (2016) 445–451, https://doi.org/10.1016/j.eurpolymj.2016.10.052.
[36] R. Mejri, J. Dias, S.B. Hentati, M. Martins, C. Costa, S. Lanceros-Mendez, Effect of anion type in the performance of ionic liquid/poly (vinylidene fluoride) electromechanical actuators, J. Non-Cryst. Solids 453 (2016) 8–15, https://doi.org/10.1016/j.jnoncrysol.2016.09.014.
[37] J. Dias, A. Lopes, B. Magalhães, G. Botelho, M.M. Silva, J. Esperança, S. Lanceros-Mendez, High performance electromechanical actuators based on ionic liquid/poly (vinylidene fluoride), Polym. Test. 48 (2015) 199–205, https://doi.org/10.1016/j.polymertesting.2015.10.012.
[38] S. Guo, L. Shi, K. Asaka, IPMC actuator-sensor based a biomimetic underwater microrobot with 8 Legs, in: 2008 IEEE International Conference on Automation and Logistics, IEEE, 2008, pp. 2495–2500, https://doi.org/10.1109/ICAL.2008.4636588.